Available online at www.sciencedirect.com

ScienceDirect

Procedia CIRP 141 (2026) 544–549

www.elsevier.com/locate/procedia

10th Conference on High Performance Cutting (CIRP-HPC 2026)

A comparative study of tool wear behavior for PVD coatings with different functional layers

Benjamin Bergmann[a], Nico Junge[a]*, Christian Kalscheuer[b], Kirsten Bobzin[b], Xiaoyang Liu[b], Vanessa K. J. Weißbrodt[c], Hans J. Maier[c]

[a]*Institute of Production Engineering and Machine Tools, An der Universität 2, 30283 Garbsen, Germany*
[b]*Surface Engineering Institute, Kackertstr. 15, 52072 Aachen, Germany*
[c]*Institute of Materials Science, An der Universität 2, 30823 Garbsen, Germany*

* Corresponding author. Tel. +49-511-762-18380; fax: +49-511-762-5115. *E-mail address:* junge@ifw.uni-hannover.de

Abstract

To maximize the wear resistance of high-performance cutting tools, hard coatings are applied by using Physical Vapor Deposition (PVD). Beyond the specific cutting conditions, the coating composition and the resulting coating properties are decisive factors influencing the performance of the cutting tool. This paper investigates the effects of different functional layers and the resultant coating properties on the wear behavior of the cutting tools during turning of C45+N steel. Therefore, cutting tools based on WC-Co substrate with 6 wt.% Co are coated with TiAlCrN, TiAlSiN, and TiAlCrSiN. A comprehensive coating characterization was conducted, including the measurement of residual stresses by focused ion beam combined with digital image correlation. The coated tools were used in turning experiments to determine the tool wear behavior of the different coatings. Among the coatings the TiAlCrN coating demonstrated the longest tool life. This study aims to establish a connection between coating properties with a focus on the residual stresses and wear behavior of different coating compositions.

Peer-review under responsibility of the scientific committee of the 10th Conference on High Performance Cutting (CIRP-HPC 2026)

Keywords: pvd; coatings; tool wear; cutting; residual stresses

1. Introduction

Cemented carbide tools are the most common choice for high-performance cutting applications [1]. To enhance their wear resistance and facilitate the use of more aggressive cutting parameters, hard coatings are applied by using Physical Vapor deposition (PVD). In this context, TiAlN-based coatings have proven to be effective [2]. The increasing demand for productivity drives the development of more complex coating systems, such as TiAlSiN, TiAlCrSiN, and TiAlCrN. The addition of Si can facilitate the formation of a nanocomposite structure, where TiAlN crystallites are embedded in an amorphous Si_3N_4 matrix as described in [3,4]. Nanocomposite TiAlSiN coatings are characterized by increased hardness, improved thermal stability, and enhanced oxidation resistance. The incorporation of Cr into TiAlN to form TiAlCrN has significantly improved tool life compared to TiAlN when machining hardened steel due to superior high-temperature mechanical properties [5]. In previous work of Bobzin et al., a TiAlCrSiN coating was deposited on cutting inserts, which demonstrated good wear behavior in cutting experiments [6]. To gain deeper insight into the underlying mechanism of this

2212-8271
Peer-review under responsibility of the scientific committee of the 10th Conference on High Performance Cutting (CIRP-HPC 2026)
10.1016/j.procir.2026.03.016

coating system and to further develop the coating, the effects of Si and Cr are investigated separately.

A decisive factor for tool wear behavior is the presence of residual stresses. Compressive residual stresses in PVD coatings can substantially increase the coating's mechanical properties and adhesion, which, in turn, can significantly prolong tool life [7]. Based on previous research of Breidenstein et al, one of the factors influencing the residual stresses, in addition to the substrate pretreatment is the coating composition [8,9].

In this study, the original TiAlCrSiN coating, which features the addition of both Cr and Si to the TiAlN crystallites, is evaluated against its two variants, TiAlSiN coating adding only Si to TiAlN and TiAlCrN coating adding only Cr. These coatings are first deposited and characterized, with special attention paid to the difference in their compressive residual stress. Subsequently, cutting experiments are conducted to evaluate tool wear behavior.

2. Experimental setup

2.1 Coating deposition

All three coating types were deposited on WC-Co substrates with 6 wt.% Co and CNMA 120404 geometry supplied by CERATIZIT GmbH, Luxembourg. The industrial CC800/9 HPPMS coating unit from CemeCon AG, Würselen, Germany, was used for the coating deposition. For the deposition of the TiAlCrSiN coating, two high power pulsed magnetron sputtering (HPPMS) power supplies and two direct current magnetron sputtering (dcMS) power supplies were employed. All coatings were deposited on a TiAlCrN interlayer. The process parameters and target configuration for the deposition of three different functional layers are listed in Table 1.

Table 1. Process parameters used for the deposition of three functional layers.

Process parameter	Unit	TiAlCrSiN	TiAlSiN	TiAlCrN
Process gas		Ar	Ar	Ar
Reactive gas		N_2	N_2	N_2
Argon flow Q(Ar)	mL/min	200	200	200
Nitrogen flow $Q(N_2)$	mL/min	Pressure controlled	Pressure controlled	Pressure controlled
Pulse frequency f	Hz	2000	2000	2000
Pulse on time t_{on}	µs	60	60	60
Pressure p	mPa	520	520	520
Substrate bias U_B	V	-80	-80	-80
Heating power P_H	W	8800	8800	8800
Power HPPMS $P_{HPPMS\text{-}TiAl48}$	W	7000	7000	7000
Power HPPMS $P_{HPPMS\text{-}TiAl20}$	W	7000	7000	7000
Power dcMS-Cr $P_{dcMS\text{-}Cr}$	W	300	0	300
Power dcMS-Si $P_{dcMS\text{-}Si}$	W	600	600	0

2.2 Coating characterization

The coating morphology and the coating thickness were analyzed using scanning electron microscopy (SEM), Zeiss DSM 982 Gemini, Carl Zeiss AG, Oberkochen, Germany, at central facility of electron microscopy (GFE), RWTH Aachen University, where the chemical composition was determined using energy dispersive X-ray spectroscopy (EDX). The arithmetical mean roughness R_a and the total height profile R_t were determined using confocal laser scanning microscopy (CLSM), VKX 210, Keyence Corporation, Japan. The adhesion properties between coatings and substrates were first qualitatively determined using the Rockwell-C indentation test following DIN 4856 with an indentation force of around $F \approx 588.4N$ on a HP100 Rockwell tester, KNUTH Machine Tools GmbH, Wasbek, Germany. Then the adhesion properties were quantitively analysed using scratch test following DIN EN ISO 20502:2016 on a HPG 200/2 scratch tester produced by Gesellschaft für Fertigungstechnik and Entwicklung Schmalkalden, Germany. During the adhesion tests a diamond indenter with Rockwell-C geometry was slid across the coated sample under external load. The reduced modulus E_r and indentation hardness H_{IT} were measured by nanoindentation tests using a TI950 Triboindenter from Bruker Corporation, Billerica, Massachusetts, USA. A Berkovich indenter was used for the measurement, and the values were calculated using the Oliver-Pharr method [10]. For each coating, 15 measurements were done on a polished sample.

2.3 Residual stress analysis

The residual stresses in the coatings were determined using focused ion beam (FIB) milling combined with digital image correlation (DIC) technique, following the procedure described in [11]. The measurements were carried out using an Auriga dual-beam scanning electron microscope, Carl Zeiss AG, Oberkochen, Germany. Digital image correlation was performed using VIC-2D 2009 software from Correlated Solutions, Irmo, South Carolina, USA.

A four-step procedure was applied for the determination of residual stresses using the FIB-DIC-technique (Fig. 1). Initially, a high-resolution SEM image (SE-contrast) of the surface prior to FIB-milling was acquired (a,b). Then, a circular trench was milled into the coating, causing residual stress relaxation in the ring-core and associated elastic surface displacements (c). A ring diameter of approximately 8 µm and a trench depth of d = 4 µm were employed. With these dimensions, the displacement on the surface is caused by a complete elimination of residual stresses. The coatings exhibit a thickness of approximately s = 3 µm. In all SEM images, the interface between coating and substrate was resolved. After FIB-milling a second image of the same region was taken (d) [11].

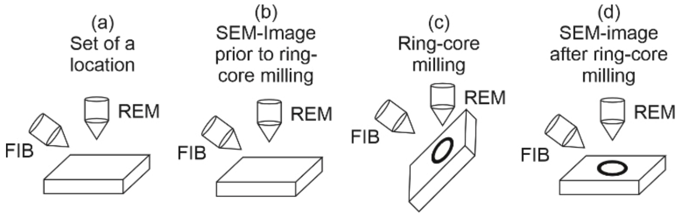

Fig. 1.Schematic steps of the ring-core milling [12].

Displacement fields were calculated through a correlation of the image pair using DIC. From the resulting in-plane strain components (ε_{xx}, ε_{yy} and ε_{xy}) the principal strains ε_1 and ε_2 can be determined according to (1). Assuming in-plane stress condition and isotropic linear elasticity, the principal residual stresses σ_1 and σ_2 were calculated as shown in (2). The elastic modulus *E* for each coating was calculated from the measured reduced modulus E_r from nanoindentation using (3). For this conversion, the elastic properties of the diamond were set to E_i = 1140 GPa and ν_i = 0.07. The Poisson's ratio of the nitride coatings was assumed to be ν = 0.25, consistently with previously reported values in [13].

$$\epsilon_{1,2} = \frac{\epsilon_{xx} + \epsilon_{yy}}{2} \pm \sqrt{\left(\frac{\epsilon_{xx} - \epsilon_{yy}}{2}\right)^2 + \left(\frac{\epsilon_{xy}}{2}\right)^2} \quad (1)$$

$$\sigma_1 = \frac{E}{1-\nu^2}(\varepsilon_1 + \nu\varepsilon_2),\ \sigma_2 = \frac{E}{1-\nu^2}(\varepsilon_2 + \nu\varepsilon_1) \quad (2)$$

$$\frac{1}{E_r} = \frac{1-\nu^2}{E} + \frac{1-\nu_i{}^2}{E_i} \quad (3)$$

2.4 Cutting experiments

The turning experiments were performed on a Gildemeister CTX 520 L lathe. The workpiece material was C45+N with a diameter D = 200 mm and a length of L = 200 mm. The process parameters were set according to Table 2. The rake angle was set to γ = -6° and the clearance angle to α = 6°. Tool wear was analyzed by using the optical microscope VHX-970 from Keyence. The width of flank wear land VB_{max} was measured according to ISO 3685. The experiments were repeated twice for each coating to confirm the results.

Table 2. Process parameters for the cutting experiments.

Process parameter	Unit	Value
Cutting speed v_c	m/min	250
Depth of cut a_p	mm	1
Feed f	mm	0.2

3. Results

3.1 Coating characterization

The morphology of the three coatings with different functional layers is shown in Fig. 2.

Fig. 2. Morphology of coatings with different functional layers.

The coating properties are summarized in Table 3. Compared to functional layers, the TiAlCrN interlayer has higher Cr concentrations.

Table 3. Coating characterization of three different coatings

Coating	Unit	Interlayer	TiAlCrSiN	TiAlSiN	TiAlCrN
Thickness s	µm	0.5	3	2.9	2.9
Ti x(Ti)	at. %	39.2	33.3	36.2	38.9
Al x(Al)	at. %	41.3	55.2	57.8	56.1
Cr x(Cr)	at. %	19.5	5.6	0	5
Si x(Si)	at. %	0	5.9	6	0
Ra	µm	0.02	0.03	0.03	0.03
Rt	µm	0.24	0.38	0.34	0.30

The adhesion properties of samples with these three different functional layers are shown in Table 4. All samples achieve a HF1 rating in the Rockwell test. In the further quantitative analysis using the scratch test, three critical loads are evaluated. The first critical load L_{c1} indicates the first appearance of cracks. The second critical load L_{c2} shows the point at which coating delamination happens. The third critical load L_{c3} marks the complete coating delamination. The results show that TiAlCrN coating contains the best adhesion properties. TiAlCrSiN and TiAlSiN samples show coating delamination at loads L_{c2} < 100 N. In contrast, the TiAlCrN sample shows the first coating delamination until L_{c2} = 130 N.

Table 4. Adhesion strength of coatings with different functional layers.

Coating	Unit	TiAlCrSiN	TiAlSiN	TiAlCrN
HF	[-]	1	1	1
Critical load L_{c1}	N	50	50	75
Critical load L_{c2}	N	85	75	130
Critical load L_{c3}	N	150	95	145

The reduced modulus E_r and indentation hardness H_{IT} using Oliver-Pharr method based on nanoindentation measurements are shown in Fig. 3. In the measurements for three coatings, the maximum indentation depth for all three coatings is kept below 130 nm, which is less than 4.5% of the total coating thickness. According to the commonly used "10% rule" in nanoindentation, the substrate effect should be minor in this case. TiAlCrN has significantly higher H_{IT} and E_r than the other two coating variants with Si. TiAlCrSiN and TiAlSiN exhibit minor differences with TiAlCrSiN exhibiting slightly higher H_{IT} and E_r than TiAlSiN.

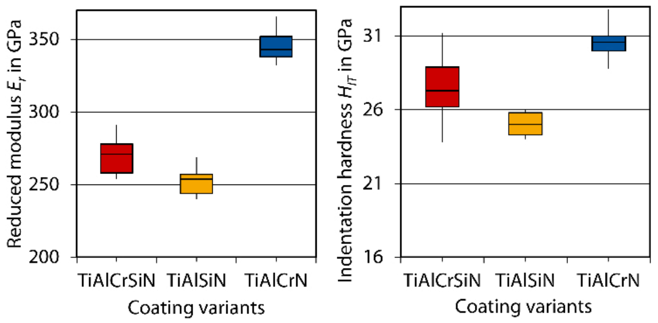

Fig. 3. Measured mechanical properties of coatings

3.2 Residual stresses

Following the FIB-milling, an expansion of the ring-core surface was observed, confirming the release of initially compressive residual stresses within the coatings. Representative strain fields obtained from FIB-DIC measurements for all three coatings are shown in Fig. illustrating the local strain component distributions on the surface of the milled ring cores. From the principal stresses, the mean residual stresses were calculated to facilitate comparison between the different coatings. The corresponding results for all three coatings, including principal and mean residual stresses, are summarized in Table 5.

An uncertainty estimation was performed following the principles of [11], considering the dominant contributions arising from strain scatter, digital image correlation (DIC) accuracy, and uncertainties in the elastic constants. Strain scatter was represented by a constant contribution of $\pm 1\times10^{-4}$, while the contribution associated with DIC accuracy was taken as ±5 % of the measured strain. Uncertainties in Young's modulus were assumed to be ±5 %, and Poisson's ratio was assigned an uncertainty of ±0.02. All contributions were Type-B and therefore treated as rectangular distributions and converted to standard uncertainties using a √3 divisor. The combined standard uncertainty was calculated using the root-sum-of-squares method and expanded uncertainties were obtained with a coverage factor of k = 2, corresponding to an approximate 95 % confidence level.

All coatings exhibit compressive residual stresses, which are characteristic for sputtered PVD hard coatings. The magnitude of the mean residual stress varies resulting from the specific deposition parameters and chemical composition. The TiAlCrN coating shows the highest compressive stress level with a mean residual stress of – 1376 MPa, whereas TiAlSiN and TiAlCrSiN exhibit comparable mean values of - 402 MPa and - 397 MPa. Following the FIB-milling, an expansion of the ring-core surface was observed, confirming the release of initially compressive residual stresses within the coatings. Representative strain fields obtained from FIB-DIC measurements for all three coatings are shown in Fig. illustrating the local strain component distributions on the surface of the milled ring cores. From the principal stresses, the mean residual stresses were calculated to facilitate comparison between the different coatings. The corresponding results for all three coatings, including principal and mean residual stresses, are summarized in Table 5.

All coatings exhibit compressive residual stresses, which are characteristic for sputtered PVD hard coatings. The magnitude of the mean residual stress varies resulting from the specific deposition parameters and chemical composition. The TiAlCrN coating shows the highest compressive stress level with a mean residual stress of – 1376 MPa, whereas TiAlSiN and TiAlCrSiN exhibit comparable mean values of - 402 MPa and - 397 MPa. The VIC-2D correlation quality is quantified by the correlation confidence value, which represents the estimated sub-pixel uncertainty of the displacement solution (matching error) of the image correlation between the pre- and post-milling SEM images. Values of 0.017–0.022 px indicate a very good and spatially uniform correlation, i.e., the same surface features are consistently tracked before and after FIB milling.

Table 5. Residual stress characteristics of TiAlCrSiN, TiAlSiN, and TiAlCrN PVD-coatings obtained from ring-core FIB-DIC analysis.

Coating	Unit	TiAlCrSiN	TiAlSiN	TiAlCrN
Principal stress σ_1	MPa	-761±93	-473±63	-1878±161
Principal stress σ_2	MPa	-32±69	-331±57	-1376±122
Mean stress $\overline{\sigma}$	MPa	-397±58	-402±42	-1627±101
Correlation confidence	Px	0.017	0.017	0.022
Subset size	Px	45	45	45

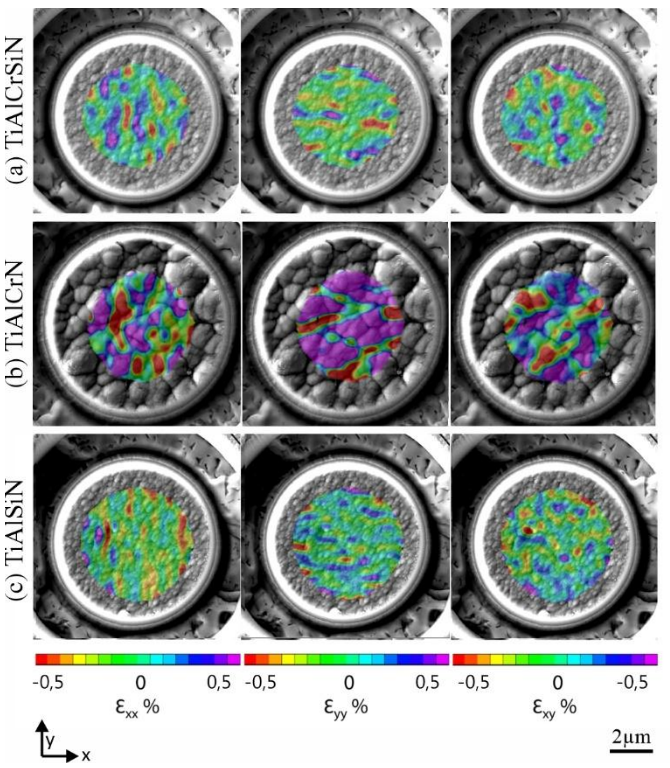

Fig. 4. In-plane strain maps (ε_{xx}, ε_{yy} and ε_{xy}) after FIB ring-core milling for (a) TiAlCrSiN, (b) TiAlCrN, and (c) TiAlSiN. Strain fields determined by DIC and overlaid on SEM images.

3.3 Tool wear analysis

In the cutting experiments, the previously characterized tools were used. Fig. 5 illustrates the rake faces of the cutting tools after a cutting time of t_c = 4 min. This time was selected as it corresponds to the last step before the first tool reached the tool life criterion. The TiAlSiN and TiAlCrSiN coated tools exhibit significant crater wear after 4 minutes cutting time. The TiAlCrN coating, however, shows no notable crater wear after the same cutting time. This higher wear resistance of the TiAlCrN tool can be attributed to higher hardness and better adhesion determined in the preceding characterization. A higher compressive residual stress might be another influencing factor. High compressive residual stresses up to a certain degree are known to enhance the mechanical properties and have a positive impact on the tool life [14,15]. In [16] compressive residual stresses of up to 3 GPa were found to have a positive influence on tool life of TiAlN-coated cutting tools. Lower and significantly higher residual stresses were not beneficial for the tool life. In comparison, there is no significant difference in the crater wear between TiAlCrSiN coating and TiAlSiN coating. The result correlates well with the comparable hardness and the compressive residual stress. The flank wear after a cutting time t_c = 4 min exhibits the same wear behavior as the crater wear. TiAlCrSiN and TiAlSiN coatings have a significantly higher width of flank wear land VB after t_c = 4 min than the TiAlCrN coating.

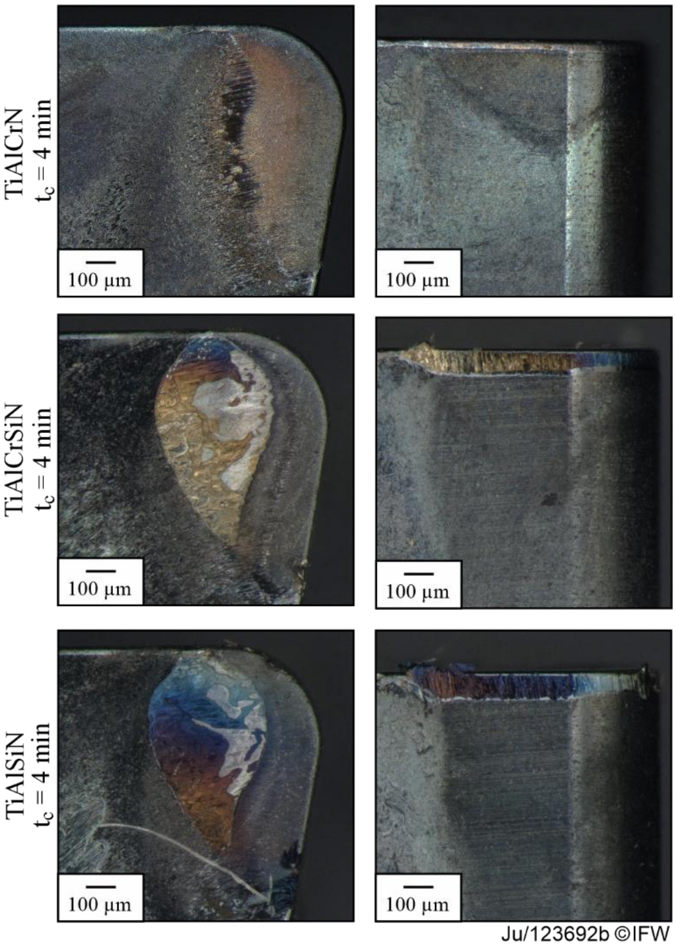

Fig. 5. wear propagation at v_c = 250 m/min after t_c = 4min.

To further examine the tool wear behavior the wear progression of the width of flank wear land VB_{max} is shown in Fig. 6. Initially, after a cutting time of t_c = 1 min, the VB_{max} values for TiAlSiN and TiAlCrSiN coatings are within a range between 65 µm and 75 µm. The width of flank wear land VB_{max} of the TiAlCrN coating after t_c = 1 min is significantly lower at 28 µm in comparison to TiAlSiN and TiAlCrSiN. Subsequently a faster increase in the width of flank wear land VB_{max} is observed for the TiAlCrSiN and TiAlSiN coating. Both tools reach the tool life criterion at VB_{max} = 200 µm after 5.5 or 6 minutes, respectively. The TiAlCrN coatings on the other hand reach the tool life criterion after a cutting time of t_c = 15 min. This equals an increase in tool life of 150%.

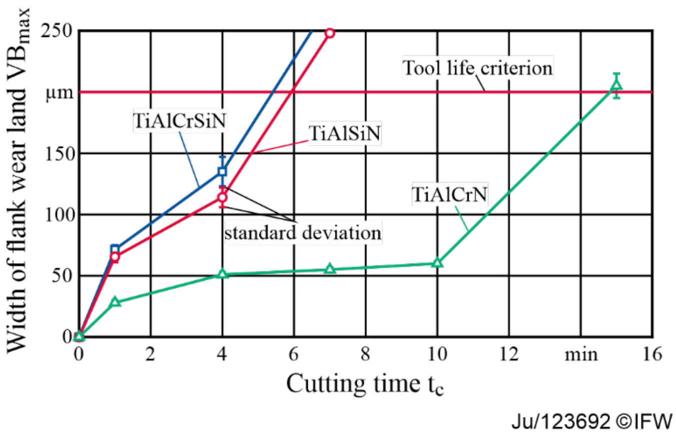

Fig. 6. Wear progression of VB_{max} for the coated cutting tools.

4. Conclusion and Outlook

Three coating variants TiAlCrN, TiAlSiN and TiAlCrSiN are deposited and characterized. The TiAlCrN coating shows the highest hardness and compressive residual stresses. The TiAlSiN coating exhibits a lower hardness and a lower compressive residual stress. The TiAlCrSiN coating combining Cr and Si is also closer to the TiAlSiN coating regarding coating properties and residual stresses. The results of the coating characterization are verified in the cutting experiments during finish turning. The better coating adhesion, higher hardness and higher compressive residual stresses of the TiAlCrN coating correlate well with increased tool life under the test condition in this work.

In future studies, a wider variation in the Si and Cr content should be examined in more detail in order to improve understanding of the influence on the coating properties, residual stresses, and the resulting wear behavior.

Acknowledgements

The authors gratefully acknowledge the financial support of the German Research Foundation, Deutsche Forschungsgemeinschaft (DFG), within KA 4899/1-1, BE 7049/4-1, project number 521383048, MA 1175/113-1, project number 521374861

References

[1] K. Bobzin, High-performance coatings for cutting tools, CIRP Journal of Manufacturing Science and Technology 18 (2017) 1–9. https://doi.org/10.1016/j.cirpj.2016.11.004.

[2] F. Klocke, T. Krieg, Coated Tools for Metal Cutting – Features and Applications, CIRP Annals 48 (1999) 515–525. https://doi.org/10.1016/S0007-8506(07)63231-4.

[3] S. Christiansen, M. Albrecht, H.P. Strunk, S. Veprek, Microstructure of novel superhard nanocrystalline-amorphous composites as analyzed by high resolution transmission electron microscopy, Journal of Vacuum Science & Technology B: Microelectronics and Nanometer Structures Processing, Measurement, and Phenomena 16 (1998) 19–22. https://doi.org/10.1116/1.589778.

[4] S. Veprek, S. Reiprich, L. Shizhi, Superhard nanocrystalline composite materials: The TiN/Si3N4 system, Applied Physics Letters 66 (1995) 2640–2642. https://doi.org/10.1063/1.113110.

[5] G.S. Fox-Rabinovich, A.I. Kovalev, M.H. Aguirre, B.D. Beake, K. Yamamoto, S.C. Veldhuis, J.L. Endrino, D.L. Wainstein, A.Y. Rashkovskiy, Design and performance of AlTiN and TiAlCrN PVD coatings for machining of hard to cut materials, Surface and Coatings Technology 204 (2009) 489–496. https://doi.org/10.1016/j.surfcoat.2009.08.021.

[6] K. Bobzin, C. Kalscheuer, M. Tayyab, T. Bergs, M. Meurer, M. Abouridouane, A case study on extended approach for wear analysis of TiAlCrSiN coated cutting inserts, Wear 572-573 (2025) 206040. https://doi.org/10.1016/j.wear.2025.206040.

[7] K.-D. Bouzakis, N. Michailidis, G. Skordaris, E. Bouzakis, D. Biermann, R. M'Saoubi, Cutting with coated tools: Coating technologies, characterization methods and performance optimization, CIRP Annals 61 (2012) 703–723. https://doi.org/10.1016/j.cirp.2012.05.006.

[8] B. Breidenstein, B. Denkena, J. Vetter, B. Richter, Influence of the residual stress state of coatings on the wear behavior in external turning of AISI 4140 and Ti–6Al–4V, Prod. Eng. Res. Devel. 10 (2016) 147–155. https://doi.org/10.1007/s11740-015-0650-7.

[9] B. Denkena, B. Breidenstein, Pre PVD-Coating Processes and their Effect on Substrate Residual Stress in Carbide Cutting Tools, KEM 438 (2010) 17–22. https://doi.org/10.4028/www.scientific.net/KEM.438.17.

[10] W.C. Oliver, G.M. Pharr, An improved technique for determining hardness and elastic modulus using load and displacement sensing indentation experiments, J. Mater. Res. 7 (1992) 1564–1583. https://doi.org/10.1557/jmr.1992.1564.

[11] J. Lord, D. Cox, A. Ratzke, M. Sebastiani, A. Korsunsky, E. Salvati, M.Z. Mughal, E. Bemporad, A good practice guide for measuring residual stresses using FIB-DIC. Measurement Good Practice Guide, The National Physical Laboratory (NPL) (2018).

[12] K. Bobzin, T. Brögelmann, N.C. Kruppe, H.J. Maier, T. Heidenblut, H.-B. Besserer, C. Kahra, J. Janowitz, 2022. CrN/AlN nanolaminates: Architecture, residual stresses, and cracking behavior. Journal of Vacuum Science & Technology A 40, 013414. https://doi.org/10.1116/6.0001462.

[13] A.J. Perry, A contribution to the study of poisson's ratios and elasticconstants of TiN, ZrN and HfN, Thin Solid Films 193-194 (1990) 463–471. https://doi.org/10.1016/S0040-6090(05)80056-2.

[14] B.Denkena, B. Breidenstein, Residual Stress Distribution in PVD-Coated Carbide Cutting Tools – Origin of Cohesive Damage, Tribology in Industry 2012 (2012) 158–165.

[15] B. Denkena, B. Breidenstein, Residual Stress Gradients in PVD-Coated Carbide Cutting Tools, MSF 524-525 (2006) 607–612. https://doi.org/10.4028/www.scientific.net/MSF.524-525.607.

[16] G. Skordaris, K.D. Bouzakis, T. Kotsanis, P. Charalampous, E. Bouzakis, B. Breidenstein, B. Bergmann, B. Denkena, Effect of PVD film's residual stresses on their mechanical properties, brittleness, adhesion and cutting performance of coated tools, CIRP Journal of Manufacturing Science and Technology 18 (2017) 145–151. https://doi.org/10.1016/j.cirpj.2016.11.003.